Hindawi
Journal of Chemistry
Volume 2017, Article ID 2346895, 9 pages
https://doi.org/10.1155/2017/2346895

Research Article

Amperometric Formaldehyde Sensor Based on a Pd Nanocrystal Modified C/Co_2P Electrode

Huan Wang,[1] Yaodan Chi,[1,2] Xiaohong Gao,[1] Sa Lv,[1] Xuefeng Chu,[1] Chao Wang,[1] Lu Zhou,[1] and Xiaotian Yang[1]

[1]*Jilin Provincial Key Laboratory of Architectural Electricity & Comprehensive Energy Saving, Department of Materials Science, Jilin Jianzhu University, Changchun 130118, China*
[2]*College of Instrumentation & Electrical Engineering, Jilin University, Changchun 130012, China*

Correspondence should be addressed to Xiaotian Yang; hanyxt@163.com

Received 20 June 2017; Revised 27 September 2017; Accepted 10 October 2017; Published 12 November 2017

Academic Editor: C. R. Raj

Ultrafine Pd nanocrystals were grown on the cobalt phosphide (Co_2P) decorated Vulcan XC-72 carbon (C/Co_2P), which is realized by first implementing the corresponding metal precursor and then the further chemical reduction process. The as-synthesized C/Co_2P/Pd composite was further constructed to form a gas permeable electrode. This electrode can be applied for formaldehyde (HCHO) detection. The results demonstrate that the Co_2P nanocrystal can significantly improve the sensing performance of the C/Co_2P/Pd electrode for catalytic oxidation of HCHO, which is considered to be attributed to the effective electron transfer from Co_2P to Pd in the C/Co_2P/Pd composites. Furthermore, the assembled C/Co_2P/Pd sensor exhibits high sensitivity of 617 nA/ppm and good selectivity toward various interfering gases such as NO_2, NO, SO_2, CO_2, and CO. It also shows the excellent linear response that the correlation coefficient is 0.994 in the concentration range of 1–10 ppm. Therefore, the proposed cost-effective C/Co_2P/Pd nanocomposite, which owns advantages such as high activity and good stability, has the potential to be applied as an effective electrocatalyst for amperometric HCHO detection.

1. Introduction

Formaldehyde, which is a colorless and toxic volatile organic compound (VOC), is an essential material that is applied in many aspects including the chemical factories and the residence decorating field. It is also well known that the formaldehyde can significantly increase the probability to get cancer for people [1]. Therefore, the detection of formaldehyde gas is significantly important. Until now, numerous technologies have been employed, such as spectrophotometry [2], gas chromatography (GC) [3], high-performance liquid chromatography [4], ion chromatography [5], polarography [6], and integrated sensor [7]. Among the above-mentioned techniques, the gas sensors have been widely reported by many research groups due to the advantages of high sensitivity, fast response, high stability, small size, and cost-effective features. In addition, these small packaged sensors can be mass fabricated easily in order to satisfy the large demand in many industrial fields. Generally, there are two types of formaldehyde gas sensor: (1) semiconductors formaldehyde gas sensor based on metal oxide such as SnO_2 [8, 9], ZnO [10], In_2O_3 [11, 12], and NiO [13] and (2) amperometric formaldehyde gas sensor made from noble metal nanomaterial, such as platinum or gold [14, 15]. In contrast with semiconductor gas sensor, the amperometric formaldehyde gas sensors have numerous advantages such as lower power consumption, excellent linear response, high sensitivity, and reasonable selectivity at room temperature.

Due to their high catalytic activity and excellent chemical stability, Pt-based catalysts are generally used in amperometric gas sensor. However, the scarcity and high cost of platinum greatly hinder its application. Much effort has been devoted to developing the platinum-free electrocatalysts, among which palladium-containing catalysts have been proven to be an effective candidate [16, 17]. The C/Pd catalyst is a good choice, due to its low cost and competitive intrinsic electrocatalytic

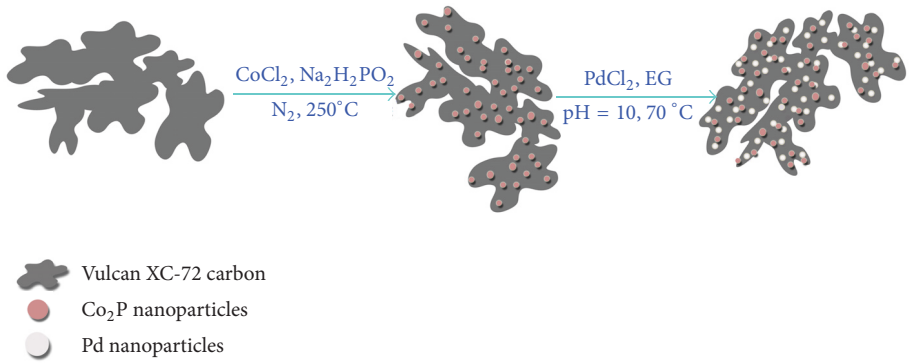

Figure 1: Synthesis procedure of Pd nanoparticle-modified C/Co_2P composites.

activity [18]. Furthermore, it is reported that the addition of another element, such as Fe, Co, Ni, N, or P, can enhance the catalytic activity of the C/Pd catalyst [19–22]. Unfortunately, the catalytic performance decreases rapidly by the dissolution or instability of the addition elements. It is well known that the transition metal phosphide nanoparticles such as Ni_2P, CoP, and FeP can significantly improve the catalytic activity and stability of catalyst [23–25]. But only a few works were reported about metal phosphide nanoparticles decorated Pd/C hybrids.

In this work, an amperometric formaldehyde gas sensor was fabricated by using the C/Co_2P/Pd catalyst as active electrode in H_2SO_4 electrolyte. The obtained C/Co_2P/Pd sensor exhibits better sensing performance for HCHO detection than that of the C/Co_2P and C/Pd sensor.

2. Experiment Section

2.1. Materials. Vulcan XC-72 carbon powder (99.9%) was purchased from Cabot Co. (USA). Sodium hypophosphite (99%), sodium hydroxide (99.9%), cobalt nitrate hexahydrate (99.99%), ethylene glycol (99.99%), ethanol (99.99%), and hydrochloric acid (37 wt.%) were purchased from Beijing Beihua Chemicals Co., Ltd. Nafion solution (5%) was purchased from DuPont Co. Palladium chloride (99.9%) was purchased from Tianjin Guangfu Chemicals Co., Ltd. Highly purified nitrogen (≥99.99%) and oxygen (≥99.99%) were supplied by Changchun Juyang Co., Ltd. Formaldehyde, nitric oxide, nitrogen dioxide, sulfur dioxide, ammonia, and carbon monoxide were supplied by Dalian Special Gases Co., Ltd.

2.2. Preparation of Co_2P Modified Pd/C Composites. Pd modified C/Co_2P composite was synthesized by solid phase reaction and ethylene glycol reduction according to a reported method [18, 23, 26, 27] and the corresponding schematic illustration is shown in Figure 1. Typically, 0.5 g Vulcan XC-72 was added to 20 mL aqueous solution containing 0.664 g $CoCl_2$. Then the mixed solution was stirred overnight followed by drying at 120°C for 5 h. The resulting Vulcan XC-72 containing $CoCl_2$ and 1.46 g $NaH_2PO_2{\cdot}H_2O$ was mechanically mixed in a quartz boat at room temperature. The precursor was directly heated to 250°C and was kept for 1 h under N_2 flowing condition. Then it was cooled to room temperature. The resulting C/Co_2P composite was passivated in a 1.0 mol% O_2/N_2 mixture for 3 h. The obtained sample was washed with deionized water and was dried at 80°C for 24 h.

The 41.6 mg $PdCl_2$ and 100 mg C/Co_2P composites were dispersed into ethylene glycol (EG, 60 ml) followed by sonicating for 1 h under ambient condition. Then the solution was further stirred for 5 h. Its pH value was adjusted to 10 by 1 M NaOH solution. Then the mixture was placed in water bath and was heated at 70°C for 3 h with vigorous stirring. After reaction, its pH value was adjusted to 3 by adding hydrochloric acid and then incubated overnight. The resulting product was collected by vacuum filtration and was washed with hot deionized water and ethanol, and the resulting C/Co_2P/Pd composites were dried at 80°C for 12 h. For comparison, the C/Pd composite was prepared under the same condition.

2.3. Preparation of Modified Electrodes. The glass carbon electrodes (GCE, d = 3 mm) surfaces were carefully polished to a mirror using alumina slurries with different diameter (1.0, 0.3, and 0.05 mm) and then thoroughly cleaned ultrasonically with ethanol and deionized water. Subsequently, 5 μL of homogeneous C/Co_2P, C/Pd, and C/Co_2P/Pd dispersion (5 mg mL^{-1}) was dropped onto the surface of GCEs, respectively. After being dried at room temperature for 24 h, three modified GCEs were obtained and denoted as C/Co_2P/GCE, C/Pd/GCE, and C/Co_2P/Pd/GCE. Each working of C/Pd and C/Co_2P/Pd electrodes contained ca. 15 μg/cm^2 of Pd.

2.4. Fabrication and Measurement of Gas Sensor. Amperometric HCHO sensor was fabricated by the method depicted in Figure 2. Circular working electrode (diameter: 1 cm, area: 0.785 cm^2) was prepared as follows: 2.0 mg of catalyst was dispersed in ethanol (0.25 mL) containing 1 μL of 0.5 wt% Nafion ethanol solution to form homogenous suspension by sonication. The mixture was sprayed onto the porous PTFE membrane (PM 28Y, Porex) and was dried at room temperature. The Pd density of the C/Co_2P/Pd electrode was 0.667 mg/cm^2. The platinum wire counter electrode and Ag/AgCl (in 3 M KCl) reference electrode were then inserted into the sensor housing. The electrolyte is 0.5 M H_2SO_4. The distances among the three electrodes are all equal to 6 cm.

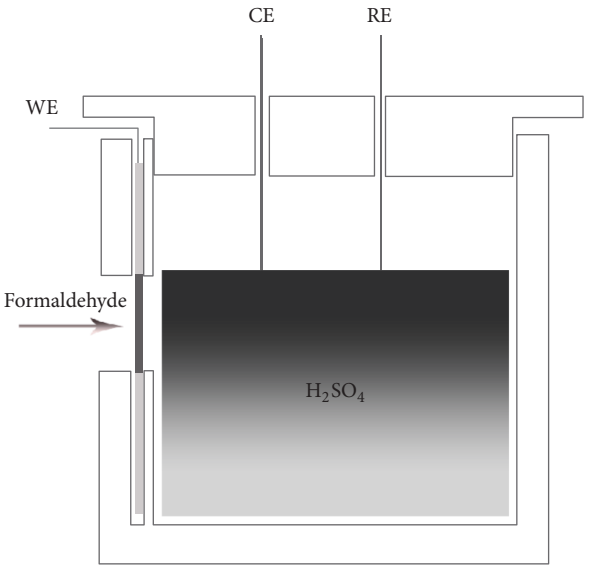

Figure 2: Schematic illustration of formaldehyde gas sensor.

2.5. Characterizations. Transmission electron microscope (TEM), high-resolution TEM (HRTEM) (TEM, JOEL TEM-2010), scanning electron microscope (SEM, Phenom ProX), and energy-dispersive X-ray (EDX, Phenom ProX) were employed to inspect the morphologies and composition of samples. X-ray photoelectron spectroscopy (XPS) analysis was performed on an ESCALAB-MKII X-ray photoelectron spectrometer (VG Co.) with Al Ka X-ray radiation as the X-ray source for excitation. Cyclic voltammetric (CV) and the gas sensing properties were performed by a CHI660C electrochemical workstation (CHI). A conventional three-electrode cell comprises a modified GCE or prepared membrane as working electrode, a platinum wire as the auxiliary electrode, and Ag/AgCl (in 3 M KCl) as reference electrode. All the gas sensors were polarized in 0.5 M H_2SO_4 solution for 24 h at 0.75 V prior to amperometric measurements. Amperometric responses were measured to various gases of HCHO, NO_2, NO, SO_2, CO_2, and CO at the applied potential of 0.75 V (versus Ag/AgCl). The standard gases of HCHO, NO_2, NO, SO_2, CO_2, and CO were purchased from Dalian Special Gases Co., Ltd. The detection gas was mixed by using a mass flow controller which was linked to one N_2 chamber and a HCHO standard chamber. Different gas concentration can be obtained by modulating the mass flow controller digitally.

3. Results and Discussion

3.1. Morphology and Component Characterization. Figure 3 shows the XRD patterns of the Vulcan XC-72 carbon (a), C/Co_2P composites (b), C/Pd composite (c), and the C/Co_2P/Pd composite (d), wherein a (002) peak is observed at 24.5° from the XC-72 carbon. After solid phase reaction, the Co_2P nanoparticles are loaded on the XC-72 carbon. The major peaks at 40.7° (121), 40.9° (201), 43.2° (211), and 48.7° (031) of the C/Co_2P composites are well matched with standard Joint Committee on Powder Diffraction Standards (JCPDS) card number 32-0306 for orthorhombic Co_2P [28, 29]. The XRD

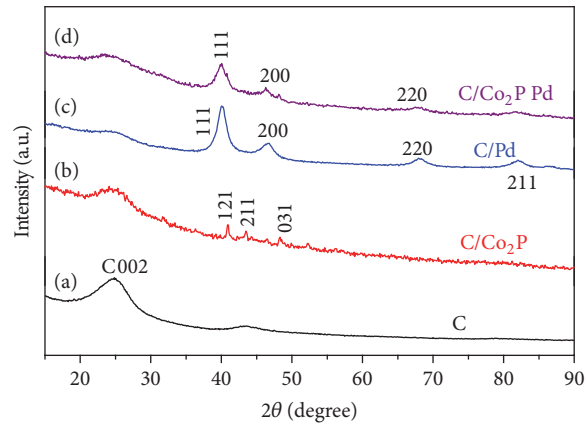

Figure 3: X-ray diffraction patterns for the Vulcan XC-72 carbon (a), C/Co_2P composite (b), C/Pd composite (c), and the C/Co_2P/Pd composite (d).

pattern of C/Pd clearly shows the peaks of metallic state Pd (JCPDS file: 65-2867) (Figure 3(c)). The XRD pattern of the C/Co_2P/Pd composite (Figure 3(d)) indicates the successful deposition of Pd nanoparticles by comparison with that of C/Pd (Figure 3(c)). However, the peaks of Co_2P are not observed in the C/Co_2P/Pd composite, which may be due to the Pd nanoparticles coated on the C/Co_2P supporters. The presence of Co_2P was confirmed by EDX and element distribution maps, and the results are similar to the previous report [23].

Morphology and element distribution of the C/Co_2P/Pd composites were characterized by TEM, HRTEM, SEM, EDX, and elemental mapping techniques. Figures 4(a) and 4(b) show the typical TEM and HRTEM images of the C/Co_2P/Pd composites. As shown in Figure 4(b), a nanocrystal particle was indicated by a red circle having a finger lattice of 0.21 nm, which is corresponding to the Co_2P (211) lattice [28]. In addition, the distances among the adjacent lattice fringes in the crystalline regions, which are marked by green circles, are 0.23 nm. This value is agrees well with the d spacing Pd (111) plane that the literature value is 0.229 nm (JCPDS number 65-6174). In order to further illustrate the surface chemical composition of the C/Co_2P/Pd composites, XPS measurements were performed from Figures 4(c)–4(f).

As shown in Figure 4(c), the survey XPS spectrum confirms the presence of C, O, Pd, Co, and P in the Pd/Co_2P/C composites. Figure 4(d) shows the XPS spectrum of Pd_{3d} in C/Co_2P/Pd composites. Two typical peaks at around 335.2 eV and 340.4 eV were corresponding to $Pd_{3d5/2}$ and $Pd_{3d3/2}$, respectively, which are located at 335.8 and 341.2 eV for the C/Pd composite (Figure S1) [30]. Such significant shift indicates a partial electron transfer from Co_2P to Pd [23]. This would increase the electron density of Pd. The unobvious peaks of P_{2p} and Co_{2p} are ascribed to Co_2P in the C/Co_2P/Pd composites, indicating the low content of the Co and P element on the surface of the C/Co_2P/Pd composites.

Figure 5 shows SEM image (a), element mapping images (b)–(f), and EDX spectrum (g) of the C/Co_2P/Pd composites. SEM image indicates that the obtained C/Co_2P/Pd

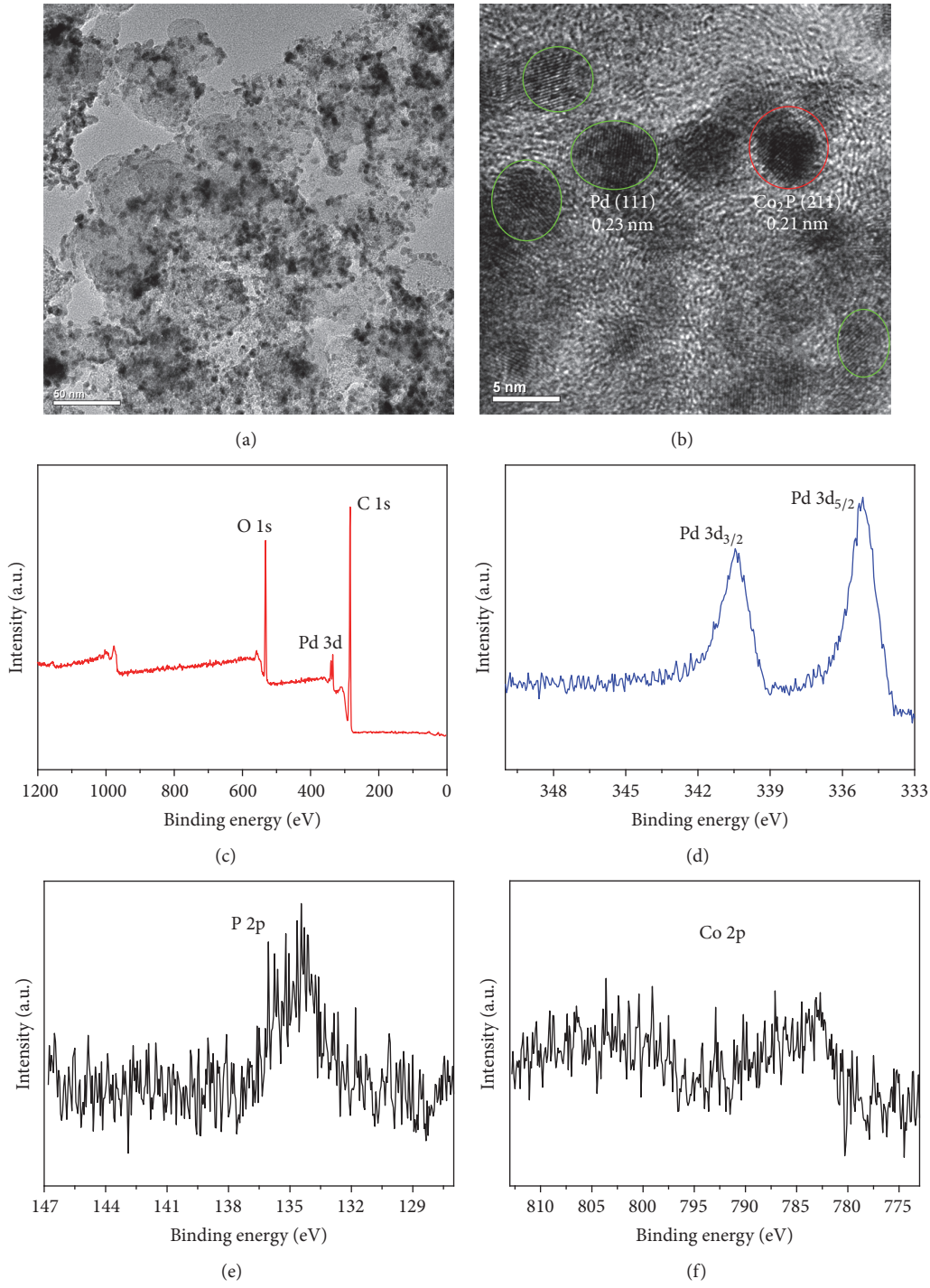

Figure 4: The TEM (a), HRTEM (b), and the survey, Pd 3d, P 2p, and Co 2p XPS spectra (c)–(f) of the $C/Co_2P/Pd$ composites.

composites are assembled of nanoparticles. As shown in Figures 5(b)–5(f), the element distribution of the $C/Co_2P/Pd$ composites was investigated by the element mapping, which clearly reveals the existence of C, Pd, O, Co, and P element in the $C/Co_2P/Pd$ composites. This result is coincident with the XPS spectra of the $C/Co_2P/Pd$ composites. Furthermore, EDX spectrum confirms the presence of C, O, Pd, Co, and P in the $Pd/Co_2P/C$ composite.

3.2. Electrochemical Properties of the $C/Co_2P/Pd$ Composites Electrodes. Figure 6(a) shows the cyclic voltammetry (CV) curves of the $C/Co_2P/GCE$ (A), C/Pd/GCE (B), and $C/Co_2P/Pd/GCE$ (C) in 0.5 M H_2SO_4 solution in potential range of −0.2–1.0 V. As shown in Figure 6(A), no current could be observed on the $C/Co_2P/GCE$. It can be seen that the CV curves of the C/Pd/GCE exhibited the characteristic Pd electrochemical reactions in H_2SO_4 solution,

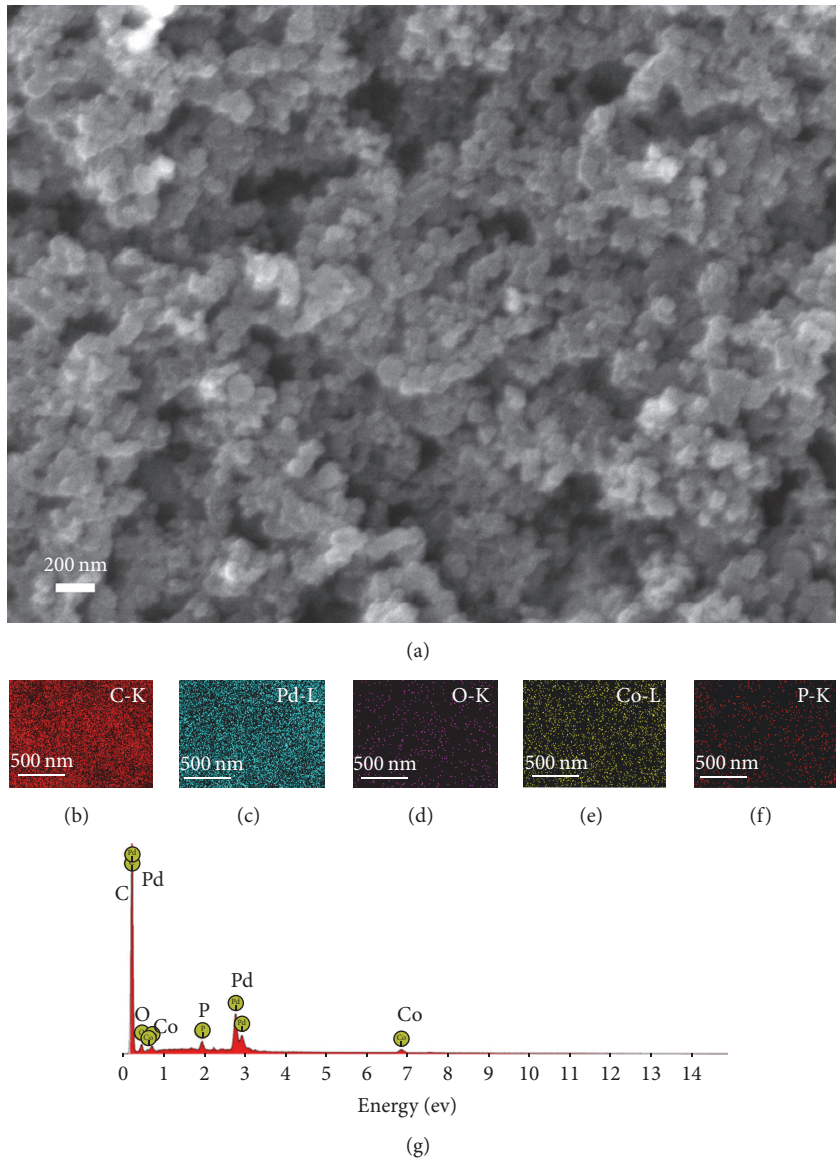

FIGURE 5: SEM image (a); element mapping images (b)–(f) for C, Pd, O, Co, and P in the C/Co_2P/Pd composites and EDX spectrum of the C/Co_2P/Pd composites.

including reversible H_{upd} region (−0.2 V–0.1 V) and Pd oxidation/reduction regions. Interestingly, compared with curve B, peak current of curve C is significantly increased, which is attributed to the strong electronic interaction between Co_2P and Pd. Figure 6(b) is the CV curve of 5 mM formaldehyde in 0.5 M H_2SO_4 solution at the C/Co_2P/Pd/GCE. In the anodic sweep from 0.2 to 0.9 V, the oxide peak appears at 0.75 V attributed to the oxidation of CO_{ads} intermediate to CO_2 on Pd surface during the formaldehyde oxidation. In the successive cathodic sweep, the current peak observed at 0.38 V was due to the reduction of palladium oxide [31].

In order to compare the catalytic activity of the C/Co_2P/GCE, C/Pd/GCE, and C/Co_2P/Pd/GCE, CVs of 50 mM formaldehyde in 0.5 M H_2SO_4 solution at the three electrodes were measured, which are shown in Figure 7(a). It is found that the C/Co_2P/Pd/GCE exhibits the relative negative oxidation potential and large current response for a given formaldehyde concentration, indicating that the C/Co_2P/Pd/GCE has much higher catalytic activity toward the oxidation of formaldehyde than C/Co_2P/GCE and C/Pd/GCE. Figure 7(b) shows CV responses of the C/Co_2P/Pd/GCE toward formaldehyde with different concentrations. It is clearly shown that the peak current of formaldehyde increases with the rise of formaldehyde concentration from 0 to 50 mM.

Figure 8(a) shows the CVs with different scan rates at the C/Co_2P/Pd/GCE in the same solution. The result reveals that as the scan rate increased, the forward oxidation peak currents increased and their peak potentials shifted slightly toward positive directions. In the case of backward potential sweep, increasing in the sweeping rate can cause the peak

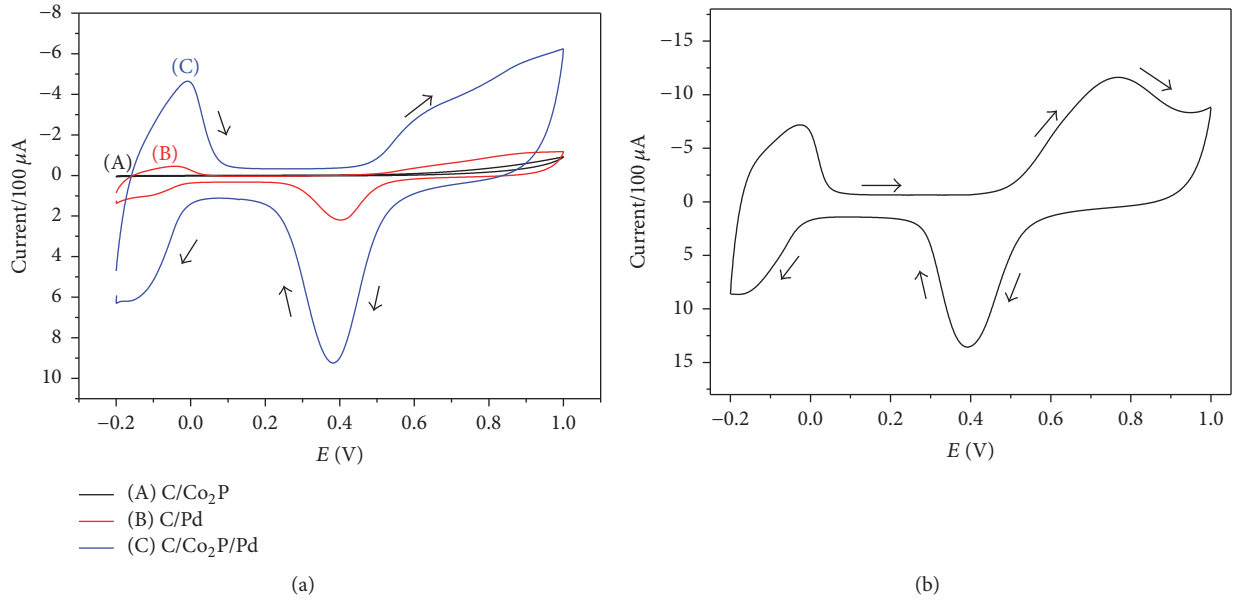

Figure 6: (a) CVs of the C/Co_2P/GCE (A), C/Pd/GCE (B), and C/Co_2P/Pd/GCE (C) in 0.5 M H_2SO_4 solution. Scan rate: 50 mV/s. (b) CV of the C/Co_2P/Pd/GCE in 0.5 M H_2SO_4 solution containing 5 mM formaldehyde from −0.2 V to 1.0 V at 50 mV/s.

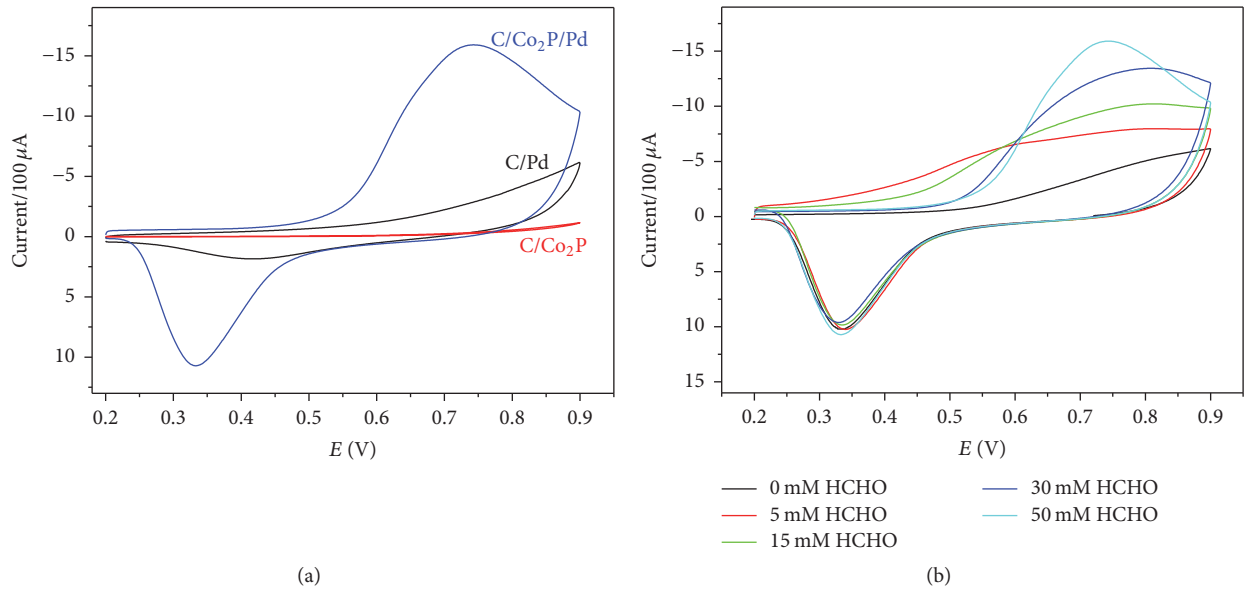

Figure 7: (a) CVs of the different electrodes in 0.5 M H_2SO_4 solution containing 50 mM formaldehyde from 0.2 V to 0.9 V at 50 mV/s. (b) CVs of the C/Co_2P/Pd/GCE in 0.5 M H_2SO_4 solution with different concentration of formaldehyde from 0.2 V to 0.9 V at scan rate of 50 mV/s.

potential to shift negatively and peak currents increased. The peak current toward formaldehyde oxidation as function of the square root of the scan rate ($v^{1/2}$) in the range of 10 to 150 mV s^{-1} is shown in Figure 8(b). A good linear relationship with correlation coefficient of 0.9985 between current response and square root of the scan rate ($v^{1/2}$) indicates a diffusion-controlled electron transfer process.

3.3. Properties of the Amperometric Gas Sensor. Figure 9(a) presents the amperometric current response of the C/Pd (black line), C/Co_2P composite (blue line), and C/Co_2P/Pd (red line) sensor. It clearly shows that the C/Co_2P/Pd sensor exhibits a higher current response than that of the C/Pd and C/Co_2P sensor. The enhanced activity of C/Co_2P/Pd may be attributed to the electron transfer from Co_2P to Pd, which was demonstrated by XPS (Figure S1 in Supplementary Material available online at https://doi.org/10.1155/2017/2346895) and previous work [23]. Typical dynamic current response for the C/Co_2P/Pd sensor was conducted under different formaldehyde concentrations (Figure 9(b)). It is seen that the peak

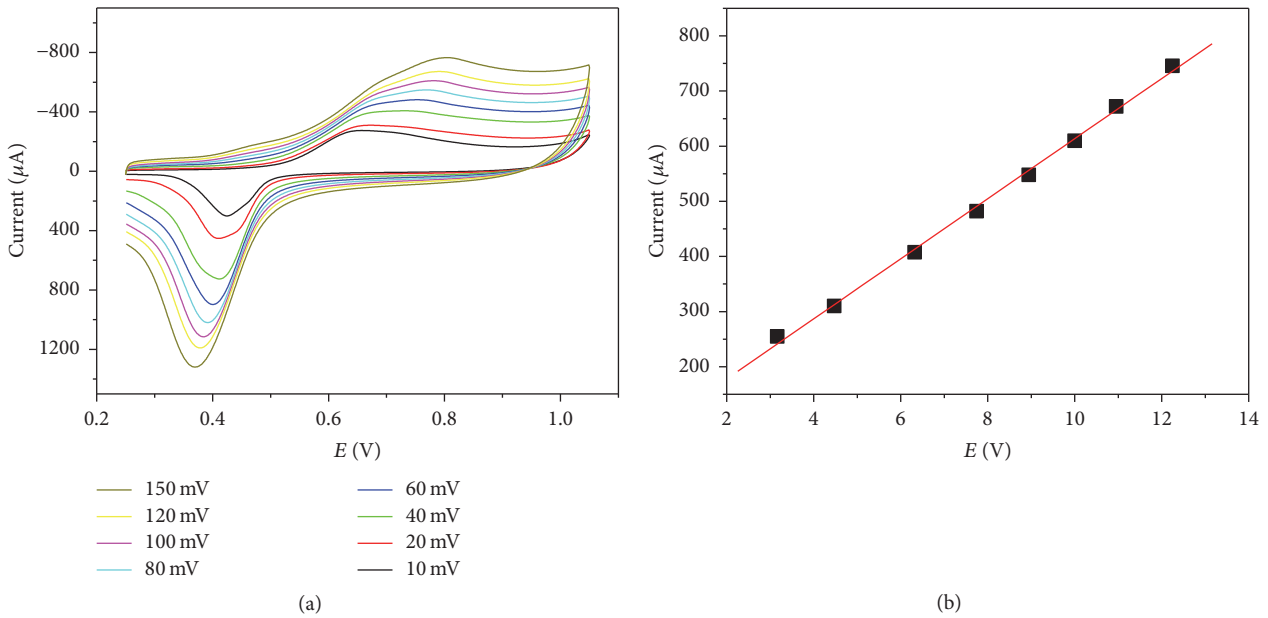

FIGURE 8: (a) CVs of the C/Co_2P/Pd/GCE in 5 mM formaldehyde of 0.5 M H_2SO_4 solution with different scan rates (10, 20, 40, 60, 80, 100, 120, and 150 mV/s). (b) The relation of the oxidation current of formaldehyde with square root of scan rate.

current increases linearly with the concentrations of HCHO from 1 to 10 ppm. The calibration curve (I (μA) = 3.57 + 5.70C (ppm); R = 0.994) was obtained from the inset of Figure 8(b), which indicates that the reaction on the C/Co_2P/Pd sensor was limited by the diffusion rate of HCHO gas [32]. On the basis of Fick's diffusion law, the limiting current I_{lim} was shown by the following equation [33]:

$$I_{lim} = k\,[\mathrm{HCOH}]_{gas}\,, \quad (1)$$

where the current is directly proportional to the gaseous concentration. It further indicates that the response is under the diffusion control at steady state.

Figure 9(c) is the enlarged parts of Figure 8(a). It shows that when the C/Co_2P/Pd sensor is exposed to HCHO gas, its current increases quickly, and it will quickly recover in the absence of HCHO. The response and recovery time are 3.8 s and 23.1 s, respectively, which are much shorter than those of the C/Pd and C/Co_2P sensor. The sensitivity of the C/Co_2P/Pd sensor is 617 nA/ppm. The background noise level is about 50 nA, which is confirmed by a previous report [34]. The limit of detection (LOD) of the C/Co_2P/Pd sensor is about 0.25 ppm (S/N = 3). The reproducibility of the HCHO gas sensor was evaluated in 10 ppm HCHO/N_2 mixture gas at six sensors prepared under the same condition. The RSD (n = 10) of the peak current is 3.25%. To evaluate the operational reproducibility of the C/Co_2P/Pd sensor, i-t curves were determined by 10 successive measurements in 10 ppm formaldehyde flow. The obtained RSD is 2.56%, which indicates that the C/Co_2P/Pd sensor can be used for routine analysis of HCHO in clinical use. The stability of the electrochemical sensor was also studied. After continuous 30 times' measurements, the current response almost does not decrease. The amperometric response with long time test for the C/Co_2P/Pd sensor was studied under continuous 10 ppm formaldehyde flow. No obvious decrease is observed in 400 s, indicating the good stability of the C/Co_2P/Pd sensor (Figure S2).

In order to investigate the selectivity of the C/Co_2P/Pd gas sensor, the amperometric measurements were performed under various testing gases such as HCHO, NO_2, NO, SO_2, CO_2, and CO. Figure 9(d) shows the current response of the C/Co_2P/Pd sensor upon exposure to 10 ppm HCHO, 10 ppm NO_2, 10 ppm NO, 10 ppm SO_2, 5000 ppm CO_2, and 50 ppm CO. The detection selectivity, defined as the relative ratio of the response current of 10 ppm HCHO to that of 10 ppm NO_2, 10 ppm NO, 10 ppm SO_2, 5000 ppm CO_2, and 50 ppm CO, was 9.3, 10.0, 33.5, 13.2, and 40.5, respectively. The as-prepared C/Co_2P/Pd sensor exhibits excellent selectivity for HCHO detection [33].

4. Conclusions

The C/Co_2P/Pd hybrids were successfully synthesized through a two-step method and further applied for fabricating a sensor for detecting HCHO. The results show that the C/Co_2P/Pd based sensor has high sensitivity of 617 nA/ppm and its LOD can be determined as 0.25 ppm. Meanwhile, it also owns a good linear response in the concentration range of 1–10 ppm. The good performance of C/Co_2P/Pd gas sensor can be analytically attributed to the fast electron transfer from Co_2P to Pd nanocrystal. The proposed work provides an alternative way for developing the cost-effective catalyst for fabricating HCHO gas sensor.

Conflicts of Interest

The authors declare that they have no conflicts of interest.

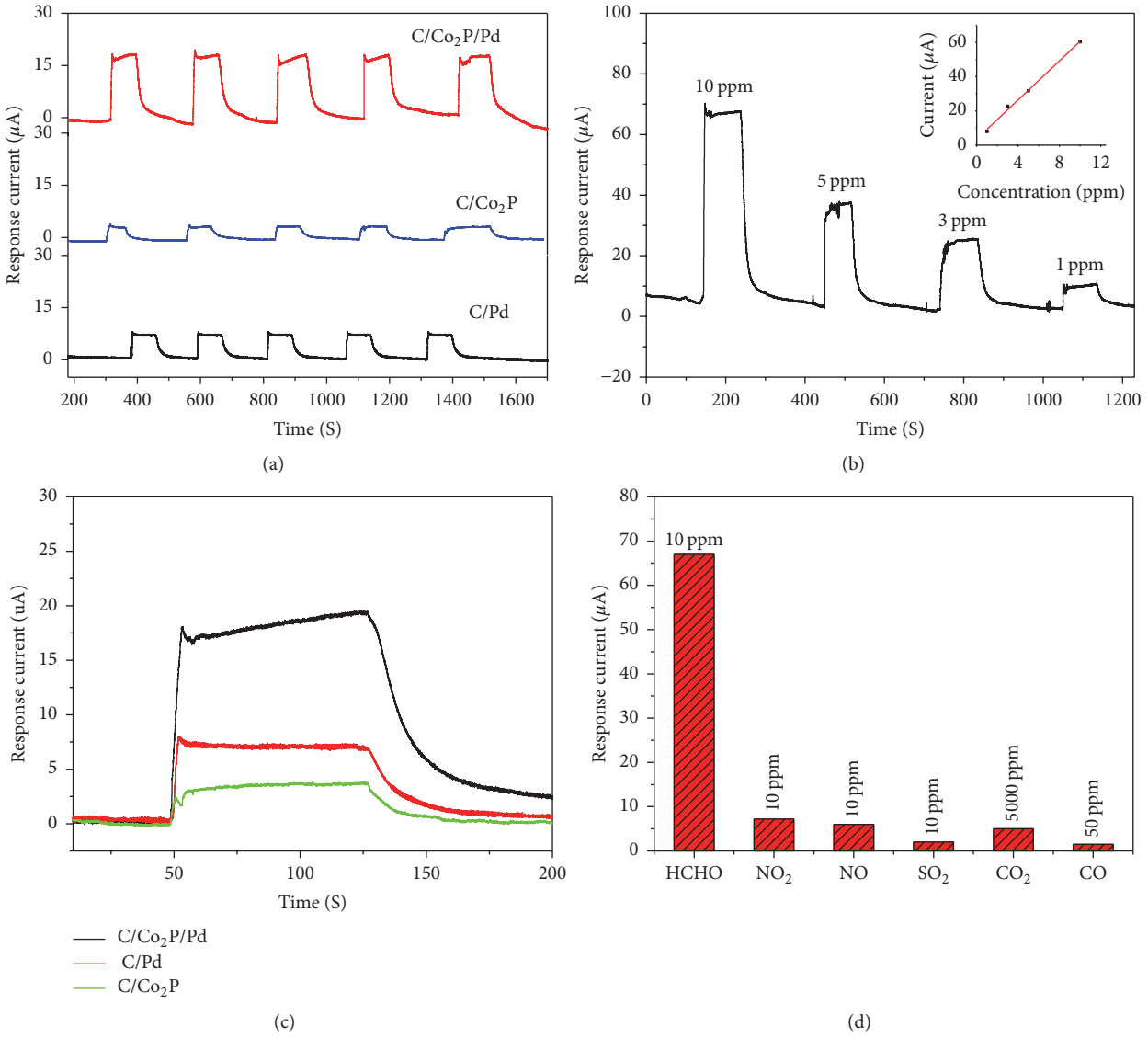

Figure 9: (a) Amperometric current responses of the C/Pd (black line), C/Co_2P composite (blue line), and C/Co_2P/Pd (red line) composites based gas sensors to 3 ppm formaldehyde. (b) Typical dynamic current response curves of C/Co_2P/Pd sensor to formaldehyde ranging from 1 ppm to 10 ppm (inset: calibration curve). (c) Enlarged part of the current responses to 3 ppm HCHO gas of the C/Pd (red line), C/Co_2P composite (green line), and C/Co_2P/Pd (black line) electrode based gas sensors. (d) Bar plot of current response of the C/Co_2P/Pd composites based formaldehyde sensor to different interfering gases under exposure to 10 ppm formaldehyde, 10 ppm NO, 10 ppm NO_2, 10 ppm SO_2, 5000 ppm CO_2, and 50 ppm CO. Applied potential to working electrode was +0.75 V (versus Ag/AgCl).

Acknowledgments

This work was supported by the National Natural Science Foundation of China (nos. 51272089, 51672103, and 21575136), National Key R&D Program of Strategic Advanced Electronic Materials (2016YFB0401103), and the Science and Technology Development Project of Jilin Province, China (nos. 20160204069GX and 20170520169JH).

References

[1] P.-R. Chung, C.-T. Tzeng, M.-T. Ke, and C.-Y. Lee, "Formaldehyde gas sensors: a review," *Sensors*, vol. 13, no. 4, pp. 4468–4484, 2013.

[2] G. R. Mohlmann, "Formaldehyde detection in air by laser induced fluorescence," *Applied Spectroscopy*, vol. 39, no. 1, pp. 98–101, 1985.

[3] T. Dumas, "Determination of formaldehyde in air by gas chromatography," *Journal of Chromatography A*, vol. 247, no. 2, pp. 289–295, 1982.

[4] B. Mann and M. L. Grayeski, "New chemiluminescent derivatizing agent for the analysis of aldehydes and ketones by high-performance liquid chromatography with peroxyoxalate chemiluminescence," *Journal of Chromatography A*, vol. 386, pp. 149–157, 1987.

[5] J. M. Lorrain, C. R. Fortune, and B. Dellinger, "Sampling and ion chromatographic determination of formaldehyde and

acetaldehyde," *Analytical Chemistry*, vol. 53, no. 8, pp. 1302–1305, 1981.

[6] J. C. Septon and J. C. Ku, "Workplace air sampling and polarographic determination of formaldehyde," *AIHAJ*, vol. 43, no. 11, pp. 845–852.

[7] B. J. Privett, J. H. Shin, and M. H. Schoenfisch, "Electrochemical sensors," *Analytical Chemistry*, vol. 82, no. 12, pp. 4723–4741, 2010.

[8] B. Kim, Y. Lu, A. Hannon, M. Meyyappan, and J. Li, "Low temperature Pd/SnO2 sensor for carbon monoxide detection," *Sensors and Actuators B: Chemical*, vol. 177, pp. 770–775, 2013.

[9] S. Tian, X. Ding, D. Zeng, J. Wu, S. Zhang, and C. Xie, "A low temperature gas sensor based on Pd-functionalized mesoporous SnO_2 fibers for detecting trace formaldehyde," *RSC Advances*, vol. 3, no. 29, pp. 11823–11831, 2013.

[10] L. Han, D. Wang, Y. Lu, T. Jiang, B. Liu, and Y. Lin, "Visible-light-assisted HCHO gas sensing based on Fe-doped flowerlike ZnO at room temperature," *The Journal of Physical Chemistry C*, vol. 115, no. 46, pp. 22939–22944, 2011.

[11] C. Dong, X. Liu, B. Han, S. Deng, X. Xiao, and Y. Wang, "Non-aqueous synthesis of Ag-functionalized In2O3/ZnO nanocomposites for highly sensitive formaldehyde sensor," *Sensors and Actuators B: Chemical*, vol. 224, pp. 193–200, 2016.

[12] X. Lai, D. Wang, N. Han et al., "Ordered arrays of bead-chain-like In_2O_3 nanorods and their enhanced sensing performance for formaldehyde," *Chemistry of Materials*, vol. 22, no. 10, pp. 3033–3042, 2010.

[13] C. Dong, Q. Li, G. Chen, X. Xiao, and Y. Wang, "Enhanced formaldehyde sensing performance of 3D hierarchical porous structure Pt-functionalized NiO via a facile solution combustion synthesis," *Sensors and Actuators B: Chemical*, vol. 220, pp. 171–179, 2015.

[14] C.-H. Chou, J.-L. Chang, and J.-M. Zen, "Effective analysis of gaseous formaldehyde based on a platinum-deposited screen-printed edge band ultramicroelectrode coated with Nafion as solid polymer electrolyte," *Sensors and Actuators B: Chemical*, vol. 147, no. 2, pp. 669–675, 2010.

[15] S. Liu, K. Hua, Y. Su, X. Lu, C. Li, and Y. J. Wang, "Application of gold hollow nanospheres in amperometric formaldehyde gas sensor," *Chinese Journal of Analytical Chemistry*, vol. 37, pp. 1092–1096, 2009.

[16] M. Yuan, A. Liu, M. Zhao et al., "Bimetallic PdCu nanoparticle decorated three-dimensional graphene hydrogel for non-enzymatic amperometric glucose sensor," *Sensors and Actuators B: Chemical*, vol. 190, pp. 707–714, 2014.

[17] Y. Jiang, Y. Lu, F. Li, T. Wu, L. Niu, and W. Chen, "Facile electrochemical codeposition of "clean" graphene-Pd nanocomposite as an anode catalyst for formic acid electrooxidation," *Electrochemistry Communications*, vol. 19, no. 1, pp. 21–24, 2012.

[18] M. Chen, Z.-B. Wang, K. Zhou, and Y.-Y. Chu, "Synthesis of Pd/C catalyst by modified polyol process for formic acid electrooxidation," *Fuel Cells*, vol. 10, no. 6, pp. 1171–1175, 2010.

[19] B. M. Leonard, Q. Zhou, D. Wu, and F. J. Disalvo, "Facile synthesis of PtNi intermetallic nanoparticles: Influence of reducing agent and precursors on electrocatalytic activity," *Chemistry of Materials*, vol. 23, no. 5, pp. 1136–1146, 2011.

[20] L. Zhang, Y. Tang, J. Bao, T. Lu, and C. Li, "A carbon-supported Pd-P catalyst as the anodic catalyst in a direct formic acid fuel cell," *Journal of Power Sources*, vol. 162, no. 1, pp. 177–179, 2006.

[21] J. Jia, R. Wang, H. Wang et al., "A novel structural design of CNx-Fe3O4 as support to immobilize Pd for catalytic oxidation of formic acid," *Catalysis Communications*, vol. 16, no. 1, pp. 60–63, 2011.

[22] X. Wang and Y. Xia, "Electrocatalytic performance of PdCo-C catalyst for formic acid oxidation," *Electrochemistry Communications*, vol. 10, no. 10, pp. 1644–1646, 2008.

[23] J. Chang, L. Feng, C. Liu, W. Xing, and X. Hu, "An effective Pd-Ni2P/C anode catalyst for direct formic acid fuel cells," *Angewandte Chemie International Edition*, vol. 53, no. 1, pp. 122–126, 2014.

[24] Z. Zhang, J. Hao, W. Yang, and J. Tang, "Defect-Rich CoP/Nitrogen-Doped Carbon Composites Derived from a Metal-Organic Framework: High-Performance Electrocatalysts for the Hydrogen Evolution Reaction," *ChemCatChem*, vol. 7, no. 13, pp. 1920–1925, 2015.

[25] J. J. Podestá, R. C. V. Piatti, and A. J. Arvia, "The influence of iridium, ruthenium and palladium on the electrochemical behaviour of Co-P and Ni-Co-P base amorphous alloys for water electrolysis in KOH aqueous solutions," *International Journal of Hydrogen Energy*, vol. 20, no. 2, pp. 111–122, 1995.

[26] X. Yang, A.-Y. Lu, Y. Zhu et al., "Rugae-like FeP nanocrystal assembly on a carbon cloth: an exceptionally efficient and stable cathode for hydrogen evolution," *Nanoscale*, vol. 7, no. 25, pp. 10974–10981, 2015.

[27] L. Song, S. Zhang, and Q. Wei, "A new route for synthesizing nickel phosphide catalysts with high hydrodesulfurization activity based on sodium dihydrogenphosphite," *Catalysis Communications*, vol. 12, no. 12, pp. 1157–1160, 2011.

[28] B. Tian, Z. Li, W. Zhen, and G. Lu, "Uniformly Sized (112) Facet Co2P on Graphene for Highly Effective Photocatalytic Hydrogen Evolution," *The Journal of Physical Chemistry C*, vol. 120, no. 12, pp. 6409–6415, 2016.

[29] M. Zuo, L. Pan, T. Sun, D. Zhao, Z. Wang, and H. Geng, "Controlled synthesis of Co2P particles with various morphologies using an in-situ melt reaction," *Materials and Corrosion*, vol. 90, pp. 858–866, 2016.

[30] M. S. Ahmed and S. Jeon, "Highly active graphene-supported NixPd100-x binary alloyed catalysts for electro-oxidation of ethanol in an alkaline media," *ACS Catalysis*, vol. 4, no. 6, pp. 1830–1837, 2014.

[31] Q. Hao and Y. Zhang, "Electrochemical degradation of formaldehyde with a novel Pd/GO modified graphite electrode," *International Journal of Electrochemical Science*, vol. 11, no. 2, pp. 1496–1511, 2016.

[32] D.-D. La, C. K. Kim, T. S. Jun et al., "Pt nanoparticle-supported multiwall carbon nanotube electrodes for amperometric hydrogen detection," *Sensors and Actuators B: Chemical*, vol. 155, no. 1, pp. 191–198, 2011.

[33] J. R. Stetter and J. Li, "Amperometric gas sensors - A review," *Chemical Reviews*, vol. 108, no. 2, pp. 352–366, 2008.

[34] M. Rashid, T.-S. Jun, Y. Jung, and Y. S. Kim, "Bimetallic core-shell Ag@Pt nanoparticle-decorated MWNT electrodes for amperometric H2 sensors and direct methanol fuel cells," *Sensors and Actuators B: Chemical*, vol. 208, pp. 7–13, 2015.